Geophysical Journal International

Geophys. J. Int. (2012) **189,** 681–690 doi: 10.1111/j.1365-246X.2012.05389.x

Interferometric imaging of the underside of a subducting crust

Oleg V. Poliannikov,[1] Stéphane Rondenay[1,2] and Ling Chen[3]

[1] *Earth Resources Laboratory, Massachusetts Institute of Technology, USA. E-mail: poliann@mit.edu*
[2] *Department of Earth Science, University of Bergen, Norway*
[3] *Institute of Geology and Geophysics, Chinese Academy of Sciences, P. R. China*

Accepted 2012 January 17. Received 2012 January 16; in original form 2011 June 16

SUMMARY

Seismic interferometry provides tools for redatuming physical data to a new source location. Turning a source, located close to a structure of interest, into a virtual receiver has the potential benefit of improving the quality of imaging by increasing the effective aperture and mitigating the effect of velocity uncertainty in the overburden. Here, we consider the problem of estimating the Green's function between two earthquakes located inside a subducting slab using earthquake data recorded at the surface. Our primary focus is to obtain an accurate time-image of the subducting interface. We propose a novel two-step kinematically correct redatuming procedure that first redatums the data from earthquakes below the subducting interface to the surface via classical interferometry, and then utilizes source–receiver wavefield interferometry to redatum virtual surface seismic data to the location of a particular earthquake event.

Key words: Interferometry; Body waves; Subduction zone processes.

1 INTRODUCTION

Seismic observations of subduction zones provide important constraints on the geological structure of the subducting slab. For example, they consistently reveal the presence of a low-velocity layer associated with the subducting crust, which is believed to be composed of hydrated metabasalts and metastable gabbro. At higher pressures, these rocks turn into higher-velocity eclogites. A high-quality seismic reflection or tomographic image with good spatial resolution will then provide important clues about the spatial extent of eclogitization. Similarly, finer resolution, higher quality images of the interfaces between the subducting crust and the overriding plate, or the subducting crust and the overriding mantle wedge, will improve our understanding of the shape and extent of the sediments and channels near the interface.

In this paper, we consider the problem of imaging the interface between the subducting crust and the overlying mantle using multiple earthquakes that have originated inside the subducting slab and have been recorded at the surface. We propose a novel algorithm to treat this problem and make a preliminary assessment of its applicability by using a synthetic data set. The 2-D numerical setup that we will use for illustration purposes is shown in Fig. 1 and is modelled after a subducting slab in Northern Japan (Chen *et al.* 2005). The numerical model is fully elastic. However, for simplicity of presentation, we will be interested only in the *P* component, and all theory will be written for the acoustic case. The model contains a line of explosive sources, which represent idealized seismicity inside the low-velocity subducting crust, and a dense receiver array at the surface where the earthquake data are recorded. The goal is to obtain a reflection image of the upper interface of the subducting crust. We note that although the problem of imaging of subducting slabs is of great interest in itself, much of what follows is general and applicable to other imaging problems where a reflector is illuminated from below.

Traditional imaging techniques, such as seismic reflection and refraction surveys (The ANCORP Working Group 1999; Preston *et al.* 2003; Calvert 2004), tomography methods (Husen *et al.* 2003; Stachnik *et al.* 2004; Zhang & Thurber 2006; Wiens *et al.* 2008) or receiver function migration (Rondenay *et al.* 2001; Chen *et al.* 2005; Abers *et al.* 2009; Suckale *et al.* 2009; MacKenzie *et al.* 2010) recover discontinuities but do not resolve fine structure of those interfaces because of potential unresolved anomalies, for example, velocity uncertainty in the overriding crust and the mantle wedge (Wagner *et al.* 2005; Shelly *et al.* 2006). Anomalies along the interface of the subducting crust could reasonably be attributed to unresolved velocity variations in the overburden. It would be ideal to put a source and a receiver as close to the interface of interest as possible to reduce the effect of the overburden on the resulting image but doing so in practice is impossible.

Seismic interferometry has been extensively employed to mitigate the effect of the velocity uncertainty by redatuming the recorded data closer to the area of interest. Following this general approach, we will construct virtual gathers at earthquake locations using surface data. Each virtual gather will contain time-images of the interfaces as if the survey had been physically conducted from within the subducting slab.

Interferometric reconstruction of the Green's function between two receiver or source locations can be done in several ways. In classical interferometry, gathers recorded at two receiver locations are correlated trace by trace and the resulting correlogram is stacked

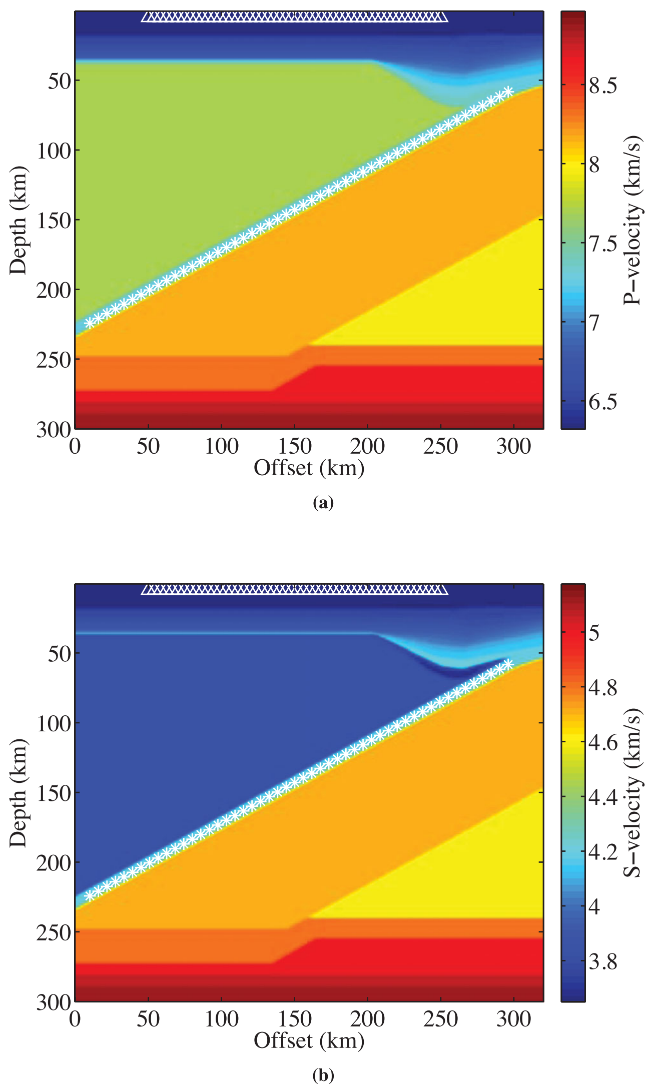

Figure 1. A numerical model with an overriding Moho (horizontal interface at the depth of about 35 km) and a subducted crust (dipping interface). Sources (marked by stars) are inside the subducting slab. Receivers (marked by triangles) are positioned on the surface.

over all sources. Under idealized assumptions, including that in which the sources completely surround the medium, a bandlimited Green's function between the receiver locations is obtained (Snieder 2004; Wapenaar 2004). By reciprocity, we can likewise reconstruct the Green's function between two sources from data recorded by an enclosing array of receivers (Curtis *et al.* 2009). When theoretical assumptions are not met, reconstructed virtual gathers contain errors, such as fake, distorted or missing events (Mehta *et al.* 2008). If an array of receivers is placed on the surface and two sources are located in the subsurface, then reflectors above the sources are hard to recover (Poliannikov 2011). Classical interferometry alone is, therefore, insufficient to achieve our goal.

Another way to recover the Green's function between two sources (or receivers) is source–receiver wavefield interferometry originally proposed by (Curtis & Halliday 2010). Unlike classical interferometry, it requires two contours of instruments: one of sources and another of receivers. With sources and receivers at the surface, it is possible to redatum surface-side reflections down to virtual receivers in the subsurface (Poliannikov 2011). Because our setup does not include shots on the surface, source–receiver wavefield interferometry also cannot be successfully employed alone.

We propose to use available earthquakes originated in the subducting slab to construct a kinematically correct approximation to the Green's function between any two such earthquakes. Amplitude effects, being extremely important in certain applications, are ignored in this particular study. The redatuming procedure consists of two steps. First, we redatum all earthquake data to the surface by classical interferometry and, by doing so, we convert surface-related Moho multiples to virtual surface seismic reflections. Then, with an array of virtual sources at the surface, we redatum the simulated surface-side reflections down to the earthquake location by source–receiver wavefield interferometry. Provided that the initial earthquakes are sufficiently strong and spread out and that a sufficiently large array of receivers is available at the surface, this process produces a virtual gather containing the underside reflections off the structures in which we are interested.

2 INTERFEROMETRY

Our goal is to image the boundary of the subducting crust. Ideally, this would be done by placing sources and receivers very close to the interface, but doing so in practice is impossible. Seismic interferometry provides a method of redatuming physically recorded earthquake data to be as if they were recorded at earthquake locations. The result of this procedure is an approximation of the gather that would have been recorded had a survey been conducted from within the subducting crust. In the next subsection, we review the existing approaches to interferometric redatuming that are critical components of the proposed new redatuming method, which is discussed in the subsequent subsection.

2.1 Classical interferometry

In classical-controlled source interferometry, two receivers are assumed to be surrounded by sources; the response from each source is recorded at both receivers. These two sets of signals are then pairwise cross-correlated and the resulting correlogram is stacked over all of the sources to form an estimate of the Green's function between the two stations (Campillo & Paul 2003; Wapenaar 2004). By reciprocity, this can also be done with two sources surrounded by receivers where one of the sources becomes a virtual receiver (Curtis *et al.* 2009, see also Fig. 2).

Mathematically, the sum of the causal and anticausal Green's function is written in the far field of the sources as

$$G(\boldsymbol{x}_{\mathrm{s},2};\boldsymbol{x}_{\mathrm{s},1}) + G^*(\boldsymbol{x}_{\mathrm{s},1};\boldsymbol{x}_{\mathrm{s},2}) \propto \int_{\boldsymbol{x}_\mathrm{r}\in\mathscr{S}} G^*(\boldsymbol{x}_\mathrm{r};\boldsymbol{x}_{\mathrm{s},1})\, G(\boldsymbol{x}_\mathrm{r};\boldsymbol{x}_{\mathrm{s},2})\,\mathrm{d}S, \tag{1}$$

where $G(\boldsymbol{x}_\mathrm{r};\boldsymbol{x}_\mathrm{s})$ here and below denotes the acoustic Green's function in the frequency domain between $\boldsymbol{x}_\mathrm{s}$ and $\boldsymbol{x}_\mathrm{r}$, $\mathscr{S}$ is the continuous contour of receivers surrounding the medium and the star denotes complex conjugation (Rickett & Claerbout 1996; Derode *et al.* 2003; Schuster *et al.* 2004; Wapenaar 2004; Wapenaar *et al.* 2005). In this framework, the wave emanating from a source located at $\boldsymbol{x}_{\mathrm{s},1}$ is recorded by the virtual receiver at the event location $\boldsymbol{x}_{\mathrm{s},2}$. The resulting integral is a virtual trace that contains reflection events with the kinematics that would be observed if a physical receiver was located at the place of the virtual one. Each reflected event in the approximate Green's function between $\boldsymbol{x}_{\mathrm{s},1}$ and $\boldsymbol{x}_{\mathrm{s},2}$ is produced by receivers around the stationary phase point where the stationary

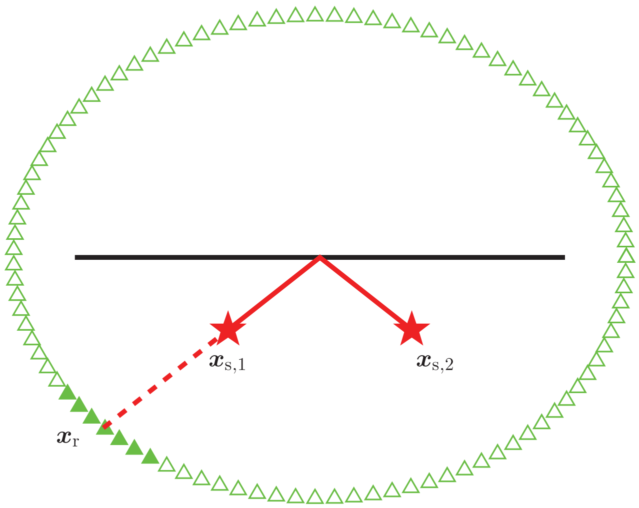

Figure 2. A cartoon description of classical interferometry. The delay time of the reflection travelling from the source, $\boldsymbol{x}_{\mathrm{s},1}$, bouncing off a reflector and received at the virtual receiver, $\boldsymbol{x}_{\mathrm{s},2}$, is computed by subtracting the direct arrival time from $\boldsymbol{x}_{\mathrm{s},1}$ (dashed line) from the time of the reflection from $\boldsymbol{x}_{\mathrm{s},2}$ recorded at the stationary phase location, $\boldsymbol{x}_{\mathrm{r}}$ (solid+dashed line).

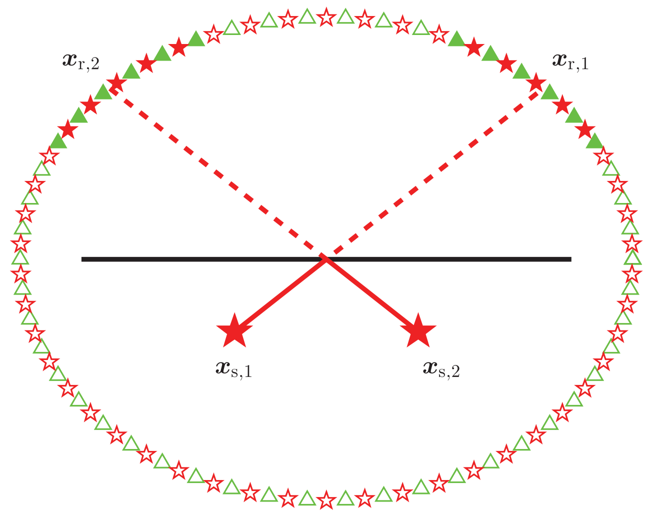

Figure 3. A cartoon description of source–receiver wavefield interferometry. The delay time of the reflection travelling from the source, $\boldsymbol{x}_{\mathrm{s},1}$, bouncing off a reflector and received at the virtual receiver, $\boldsymbol{x}_{\mathrm{s},2}$, can be computed by summing the direct traveltimes from $\boldsymbol{x}_{\mathrm{s},1}$ to $\boldsymbol{x}_{\mathrm{r},1}$ and from $\boldsymbol{x}_{\mathrm{s},2}$ to $\boldsymbol{x}_{\mathrm{r},2}$ and subtracting the boundary-side reflection time from $\boldsymbol{x}_{\mathrm{r},1}$ to $\boldsymbol{x}_{\mathrm{r},2}$ assuming the physical receiver locations, $\boldsymbol{x}_{\mathrm{r},1}$ and $\boldsymbol{x}_{\mathrm{r},2}$, are stationary. Thus, the dashed path is both added and subtracted, leaving only the solid path.

ray is received. This ray starts at the location of the second earthquake, $\boldsymbol{x}_{\mathrm{s},2}$, reflects off the structure, passes through the location of the first earthquake, $\boldsymbol{x}_{\mathrm{s},1}$ and is finally received by the stationary receivers as shown in Fig. 2. Cross-correlation and stacking remove the traveltime contribution of the part of the ray that is common to both events, and the stacking effectively cancels the contribution by other non-stationary receivers (Snieder 2004; Schuster 2009).

Although a continuous closed array of receivers surrounding the medium is required in theory (Wapenaar 2004; Schuster & Zhou 2006), the signal corresponding to the structure will also appear in the virtual gather in non-ideal setups so long as the structure is properly illuminated. In the setup shown in Fig. 2, it is sufficient to have just the receivers that are close to the stationary location (marked with filled markers) to successfully redatum the reflection from the only structure present in the model. Of course, this setup is not appropriate for earthquakes inside a subduction zone, because it requires that the receivers be in the subducting crust or lower.

2.2 Source–receiver wavefield interferometry

Let us now consider a different setup. Two sources located at $\boldsymbol{x}_{\mathrm{s},1}$ and $\boldsymbol{x}_{\mathrm{s},2}$ are surrounded by two continuous contours of instruments. Physical shots are placed along one contour and physical receivers are positioned along the other contour. Following (Poliannikov 2011) we will consider a limiting case where the two contours of instruments coincide so that there is just one contour that consists of instruments capable of acting as sources or receivers as depicted schematically in Fig. 3. Although classical interferometry can be again employed, we will present an alternative method for reconstructing the Green's function between the two sources that is based on a modification of source–receiver wavefield interferometry (Curtis 2009; Curtis & Halliday 2010). Although both types of interferometry produce similarly perfect results in the ideal case, the two methods perform quite differently when the ideal theoretical assumptions are relaxed. One method may then be preferred over the other depending on the specific geometry of the experiment.

The source–receiver wavefield interferometry reconstruction algorithm proceeds as follows. All shots, both those inside the medium as well as those along the boundary contour, are fired one by one and the resulting wavefields are recorded by all available boundary receivers. The result is three separate families of Green's functions (refer to Fig. 3): first-event-to-boundary, $G(\boldsymbol{x}_{\mathrm{r},1};\boldsymbol{x}_{\mathrm{s},1})$, where $\boldsymbol{x}_{\mathrm{r},1} \in \mathscr{S}$, second-event-to-boundary, $G(\boldsymbol{x}_{\mathrm{r},2};\boldsymbol{x}_{\mathrm{s},2})$, where $\boldsymbol{x}_{\mathrm{r},2} \in \mathscr{S}$ and boundary-to-boundary, $G(\boldsymbol{x}_{\mathrm{r},2};\boldsymbol{x}_{\mathrm{r},1})$, where $(\boldsymbol{x}_{\mathrm{r},1},\boldsymbol{x}_{\mathrm{r},2}) \in \mathscr{S}\times\mathscr{S}$. Assuming explosive sources, the Green's function between $\boldsymbol{x}_{\mathrm{s},1}$ and $\boldsymbol{x}_{\mathrm{s},2}$ can be approximately computed (Curtis 2009; Curtis & Halliday 2010; Poliannikov 2011) as

$$G(\boldsymbol{x}_{\mathrm{s},2};\boldsymbol{x}_{\mathrm{s},1}) + G^*(\boldsymbol{x}_{\mathrm{s},1};\boldsymbol{x}_{\mathrm{s},2}) \propto \iint_{\mathscr{S}\times\mathscr{S}} G(\boldsymbol{x}_{\mathrm{r},1};\boldsymbol{x}_{\mathrm{s},1})\, G(\boldsymbol{x}_{\mathrm{r},2};\boldsymbol{x}_{\mathrm{s},2})\, G^*(\boldsymbol{x}_{\mathrm{r},2};\boldsymbol{x}_{\mathrm{r},1})\, \mathrm{d}S\, \mathrm{d}S'. \tag{2}$$

As in classical interferometry, if the arrays of receivers and sources completely surround the medium then all the boundary data are redatumed to the virtual receiver. The method can also be employed in experiments that involve limited source–receiver coverage so long as the structures of interest are properly illuminated.

We observe that the traveltime between the two sources along the reflected ray is geometrically obtained by summing two direct traveltimes from the sources inside the medium to the stationary receivers at the boundary, and subtracting the time of the boundary-side reflection from one stationary receiver to another, as shown in Fig. 3. The addition and subtraction of the traveltimes are related to the convolution and correlation operations inside the right-hand side of eq. (2). When the geometry is such that all the rays involved in this computation are physically excited and then recorded, the corresponding structure will be visible in the reconstructed virtual gather. Otherwise, the structure will remain invisible.

Comparing Figs 2 and 3, we see how the choice of sources and receivers affects the reconstruction of the underside reflection between two source locations by both techniques in a homogeneous medium.

Correlation-based interferometry requires that receivers positioned below the sources are available. On the other hand, to reconstruct the reflection using the classical formulation of source–receiver wavefield interferometry given by eq. (2), one would need sources and receivers above the medium. When the setup does not include sources or receivers placed at the appropriate locations, as is the case in a subduction zone, a more sophisticated approach to redatuming is required. In the next section, we describe just such an approach.

3 REDATUMING METHOD

Recall that our goal is to construct virtual receivers at the locations of earthquakes inside the subducting slab (Fig. 1) and reconstruct the underside reflections off the interface between the subducting crust and the overlying mantle. Our setup includes physical sources inside the subducting crust and physical receivers at the surface. As was shown in the previous section, neither classical nor source–receiver wavefield interferometry can be directly employed with this setup. We, therefore, propose a new two-step hybrid algorithm for redatuming the earthquake data recorded at the surface to a virtual receiver at one of the earthquake locations. This method is particularly well-suited for imaging subduction zones because it uses the abundance of available data, both local and teleseismic, and because it relies on the source–receiver geometry possible in most subduction zones.

Our algorithm can be summarized as follows. First, we redatum earthquakes to the surface thus creating virtual surface seismic data. The virtual traces so constructed approximate wavefields that would be recorded had physical shots been fired at each of the receiver locations. Then, the virtual surface seismic survey is redatumed down into the subducting slab by an application of source–receiver wavefield interferometry. A similar type of two-step interferometric algorithm for direct waves is discussed in Curtis & Halliday (2010). Our methodology applies to scattered waves and is particularly suitable for reconstructing underside reflection as we explain in greater detail below.

3.1 Step I. Reconstructing surface-side reflections

The wave emanated by each earthquake propagates up to the surface and is recorded by all of the receivers. All earthquakes are local in our simulations but the logic fully extends to teleseisms. In what follows, we are interested in the *P*-wave exclusively. P–S converted phases are ignored and treated as artefacts for the purposes of our presentation.

Part of the *P*-wave reflects off the free surface, and on its way down it is scattered back up by encountered reflectors. Although the velocity model is complex and the backscattered P–P field is rich, it is dominated by the reflection off of the overriding Moho (Fig. 4a) and the reflection off of the subducting crust (Fig. 4b). The surface-side multiples from interfaces inside the medium are also recorded by the receivers at the surface.

We use the canonical version of classical interferometry to approximate the Green's function between pairs of surface receivers using multiple sources. Each receiver can be transformed into a virtual source by cross-correlating the direct arrivals recorded at that receiver $\boldsymbol{x}_{\mathrm{r},1}$ with the corresponding scattered field recorded at all receivers $\boldsymbol{x}_{\mathrm{r},2}$, for all available sources. The direct arrival may be separated from the rest of the wavefield recorded at $\boldsymbol{x}_{\mathrm{r},1}$ via time gating. Though this separation is not necessary in principle, it may help reduce the non-physical cross-talk resulting from uncompensated correlations due to the non-ideal illumination (Bakulin *et al.* 2007).

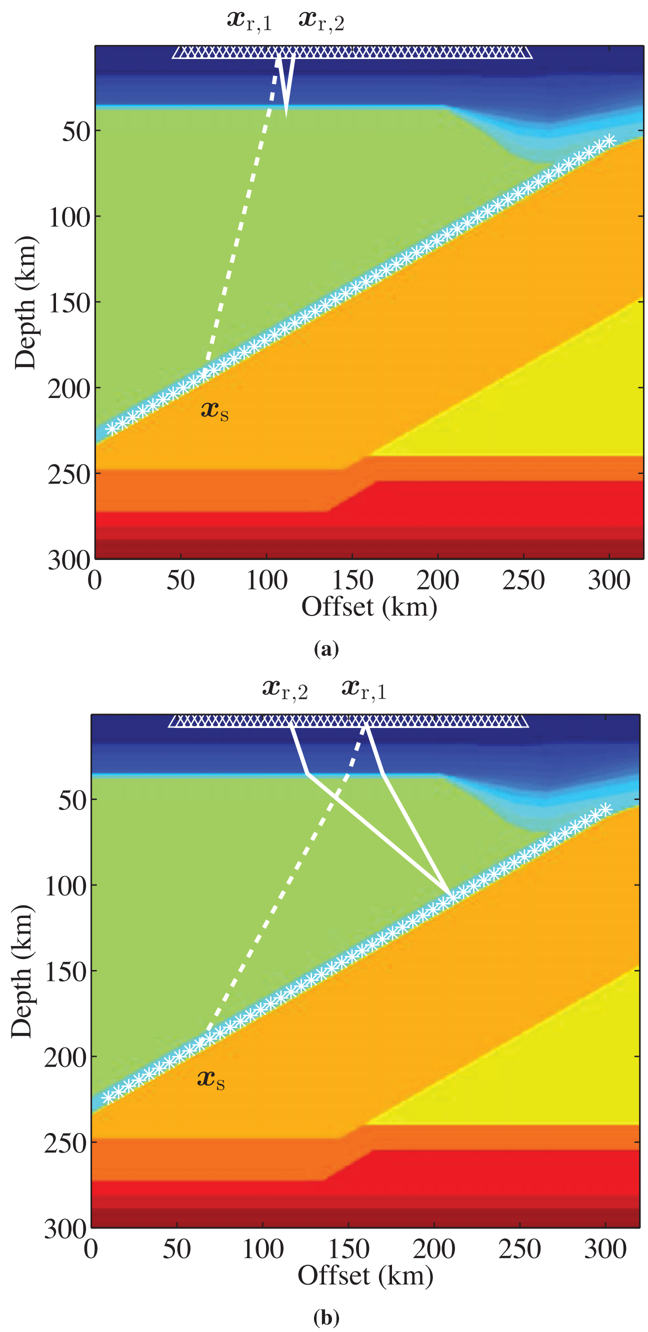

Figure 4. Recovering surface-side reflections from (a) the overriding Moho and (b) the subducted crust interface using classical interferometry. The background is the velocity. A physical source gives rise to a surface multiple, which is converted to a surface-side reflection by removing the common raypath (dashed line) with a cross-correlation.

The resulting cross-correlograms are stacked over all available sources to yield a virtual shot-gather that approximates the surface-side reflection obtained using a physical source at $\boldsymbol{x}_{\mathrm{r},1}$ and recordings at locations $\boldsymbol{x}_{\mathrm{r},2}$. We repeat the same process for all receivers $\boldsymbol{x}_{\mathrm{r},1}$ thereby constructing a virtual reflection seismic survey, with virtual sources and receivers at the surface. Fig. 5 shows an

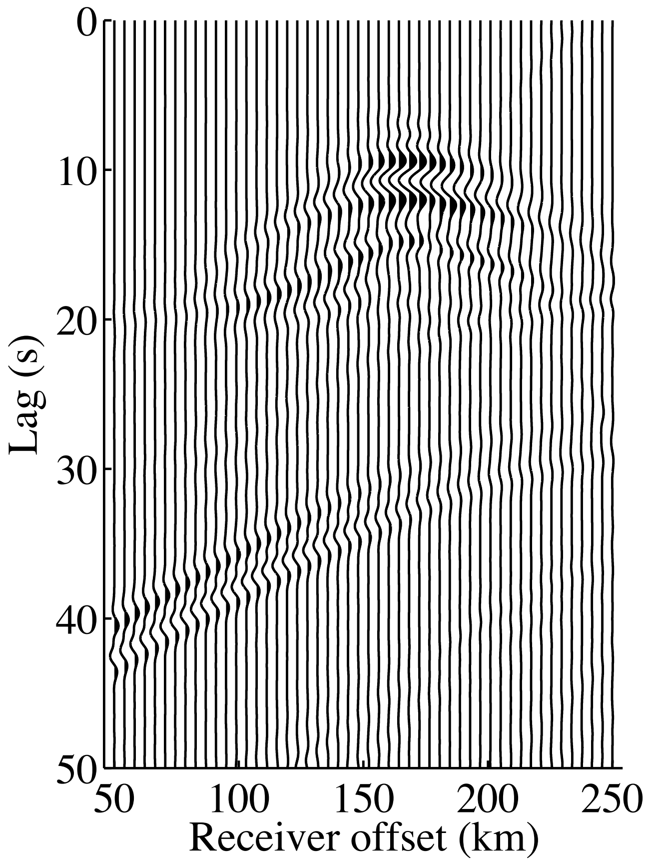

Figure 5. An example of a virtual gather reconstructed at the surface by applying classical interferometry. The virtual source is placed at offset x = 180 km. Reflections from the overriding Moho (∼10 s) and the subducted interface (∼40 s) dominate the gather.

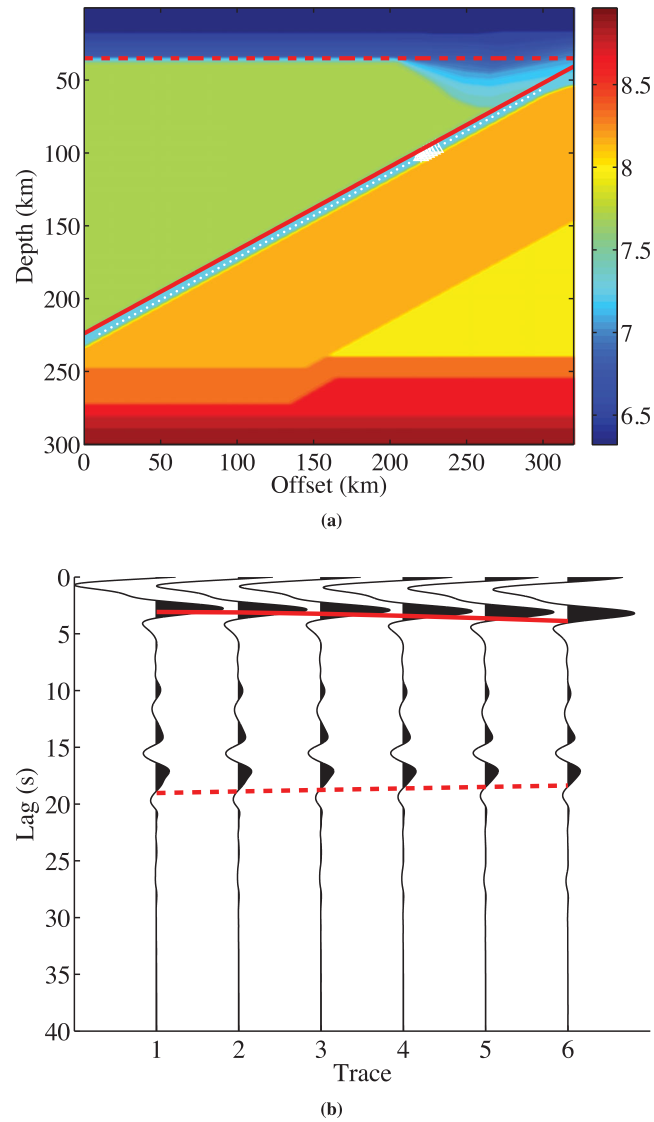

Figure 6. (a) The virtual source is placed at x = 220 km, and the virtual receivers span the offsets from 220 to 230 km. (b) The reconstructed gather is dominated by a reflection from the subducting crust (red solid line, ∼3 s). The red dashed line marks the reflection from the overriding crust. The event ∼0 s is an artefact.

example of a reconstructed (virtual) surface shot-gather for some fixed virtual source location $\boldsymbol{x}_{\mathrm{r},1}$. Reflections from the overriding Moho and from the subducting crust clearly dominate the gather. Note that the reflections from the two interfaces above and below the subducting crustal zone are not fully separated because the spatial wavelength is comparable to the width of the subducting crust.

3.2 Step II. Redatuming surface-side reflections to earthquake locations

As a result of completing the previous step, we may assume that each surface receiver shown in Fig. 1 could also be used as a source, and that those sources and receivers were used to gather (virtual) surface seismic reflection data. As was discussed in Section 2.2, this assumption is ideal for obtaining underside reflections from interfaces between any two earthquakes through source–receiver wavefield interferometry (Poliannikov 2011).

To obtain the reflections between any two given sources, $\boldsymbol{x}_{\mathrm{s},1} = (x_{\mathrm{s},1}, z_{\mathrm{s},1})$ and $\boldsymbol{x}_{\mathrm{s},2} = (x_{\mathrm{s},1}, z_{\mathrm{s},2})$, such that $x_{\mathrm{s},1} < x_{\mathrm{s},2}$, we convolve the direct arrivals from those sources, cross-correlate the result with the virtual surface reflection data and stack the resulting correlogram over all pairs of receivers $\boldsymbol{x}_{\mathrm{r},1} = (x_{\mathrm{r},1}, z_{\mathrm{r},1})$ and $\boldsymbol{x}_{\mathrm{r},2} = (x_{\mathrm{r},2}, z_{\mathrm{r},2})$, such that $x_{\mathrm{r},1} > x_{\mathrm{r},2}$. To partially deconvolve the source wavelet out of the signal, we replace the direct arrivals with delta-functions by picking traveltimes and then replacing the waveforms with spikes.

We show the results of performing this computation for three different choices of virtual gathers in Figs 6, 7 and 8. In each case the virtual gather is formed from six earthquakes, where the first earthquake is the source and all six earthquakes including the first one (zero-offset) are virtual receivers. As was noted earlier, the geometry of the stationary rays determines the ideal location for the virtual receiver depending on what structure is of interest. When the virtual gather is positioned close to the upper-right corner of the model, the subducting interface is redatumed very well (red solid line in Fig. 6). When the virtual gather is close to the lower-left corner, the overriding Moho (red dashed line in Fig. 7) is imaged very well but the subducting crust interface is not clearly visible. Finally, when the virtual gather is positioned roughly in the middle of the model, both reflectors are clearly visible (Fig. 8).

We finish this section by explaining the two artefacts that are visible in the reconstructed gathers. The first one is around 0 s and

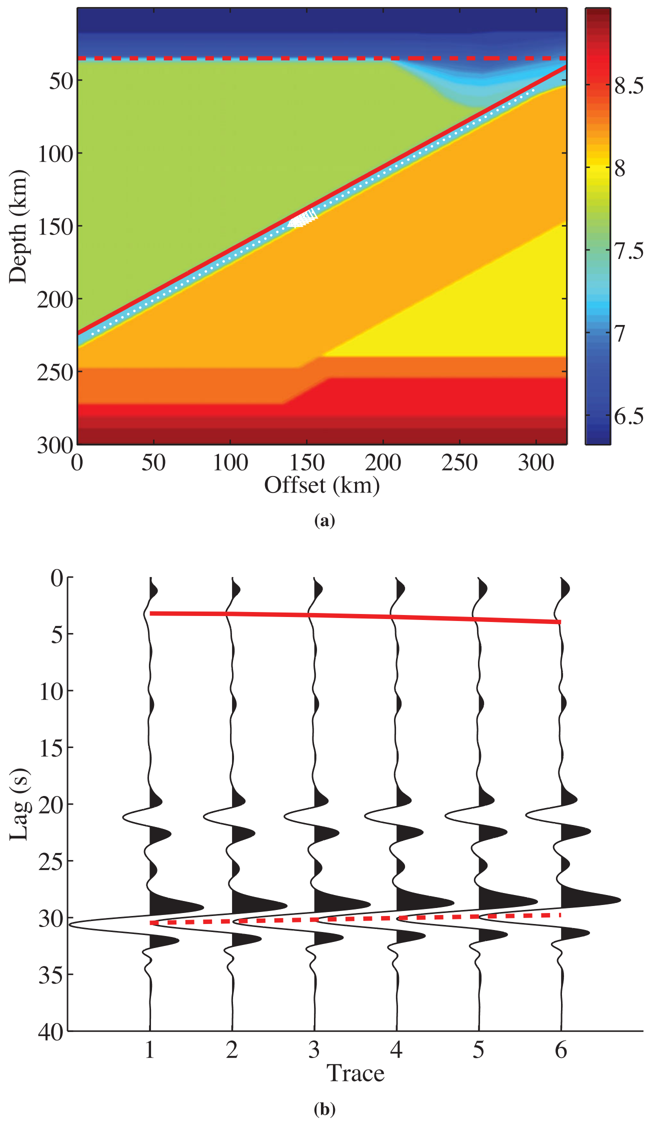

Figure 7. (a) The virtual source is placed at $x = 142$ km, and the virtual receivers span the offsets from 142 to 152 km. (b) The reconstructed gather features the reflection from the overriding Moho (red dashed line). The reflection from the subducting plate, marked by the red solid line, is not well resolved.

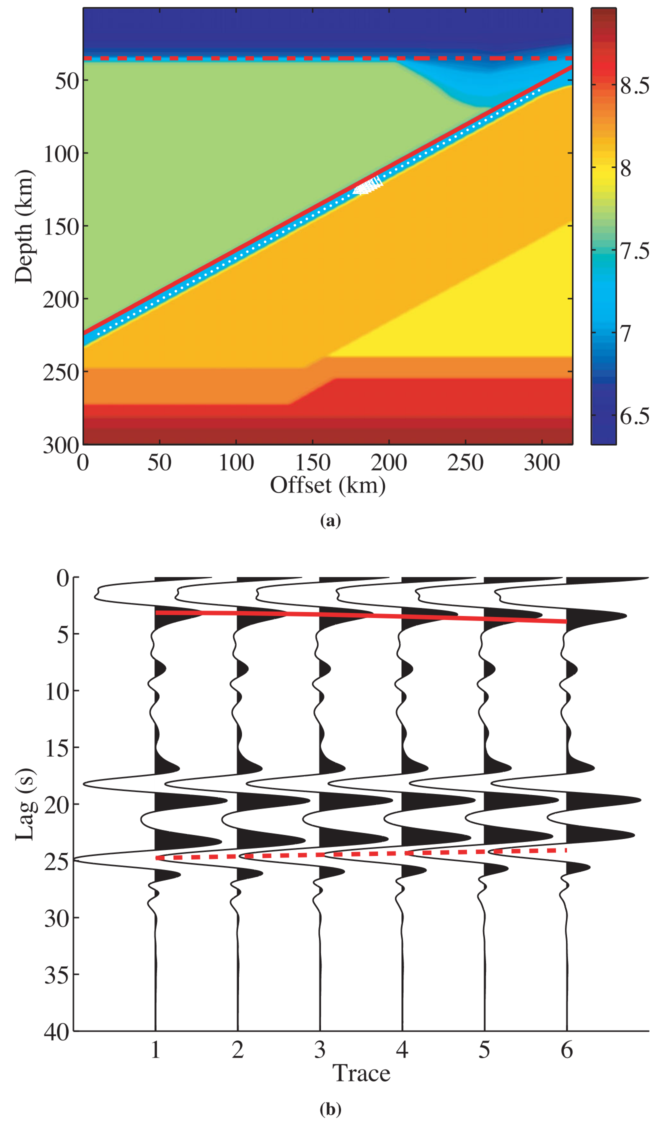

Figure 8. (a) The virtual source is placed at $x = 181$ km, and the virtual receivers span the offsets from 181 to 191 km. (b) The reconstructed gather feature the reflections from the two major interfaces: from the overriding crust (red dashed line) and from the subducting crust (red solid line). The events at ∼0 and ∼18 s are artefacts as discussed in the main text.

the second one precedes the reflection from the overriding crust at about 15–20 s. For the first artefact, recall that there are two reflectors in the vicinity of the virtual gather: one above the gather and the other one just below it. Reflections from both of these interfaces are present in the raw data as well as in the virtual seismic reflection survey constructed during Step I of the algorithm (Fig. 5). During Step II the moveout of each event is transformed according to the right-hand side of eq. (2). In the high-frequency regime, the event corresponding to the reflector above the virtual gather will have a stationary phase point and will, therefore, appear in the final stack. The event corresponding to the reflector underneath the virtual gather will have a negative moveout in the correlogram and it should appear in the final stack at a negative time. When the reflector is too close to the virtual receivers and the source frequency is too low, part of the pulse may 'leak' into the positive time half-axis.

The second artefact comes from a *P–S* conversion at the overriding crust interface during the initial propagation. In the first step of the algorithm, this phase appears in the virtual surface reflection survey as a non-physical 'reflection' (an event at ∼16 s in Fig. 5). It is, then, redatumed to the final gathers in the second step. For our purposes, we note the existence of both artefacts but proceed our analysis by ignoring them, that is, no attempt is made to remove them.

4 EFFECTS OF LIMITED SOURCE ILLUMINATION

Our numerical model contains an idealized line of sources. The illumination that these sources produce ensures the stability of the method with respect to the position of the virtual array. Although this illumination is preferred, it is not necessary for the ultimate success of the method. Here, we show that the interfaces in question can be imaged with just a small cluster of physical sources so long as the virtual receivers are correctly placed inside the subducting crust.

Both steps of the proposed redatuming algorithm are justified with the stationary phase argument. A given structure in the subsurface is successfully imaged with a fixed virtual array so long as the waves along the stationary rays, examples of which are shown in Figs 4 and 9, are excited and recorded. The event in the virtual gather that corresponds to that structure is created by a small number of sources that are inside the Fresnel zone of the stationary one. Energy emanated by the sources outside of the Fresnel zone is stacked out. If the goal is to recover not the entire virtual Green's function but just a single reflection, then a small window of near-stationary sources is sufficient. Given an approximate velocity model and the location of the virtual gather, we can verify the stationarity of available sources and, hence, the fidelity of the reconstructed event.

We show three examples of attempted redatuming using a 40 km long cluster of earthquake sources. The virtual array is set up as in Fig. 8, where both main interfaces can be seen with the full line of sources. We see that each reflection in that reference virtual gather can be recovered individually with a suitable cluster of sources. In Fig. 10, the sources are limited to offsets from 115 to 154 km but the reflection off the subducting crust is well recovered. If the

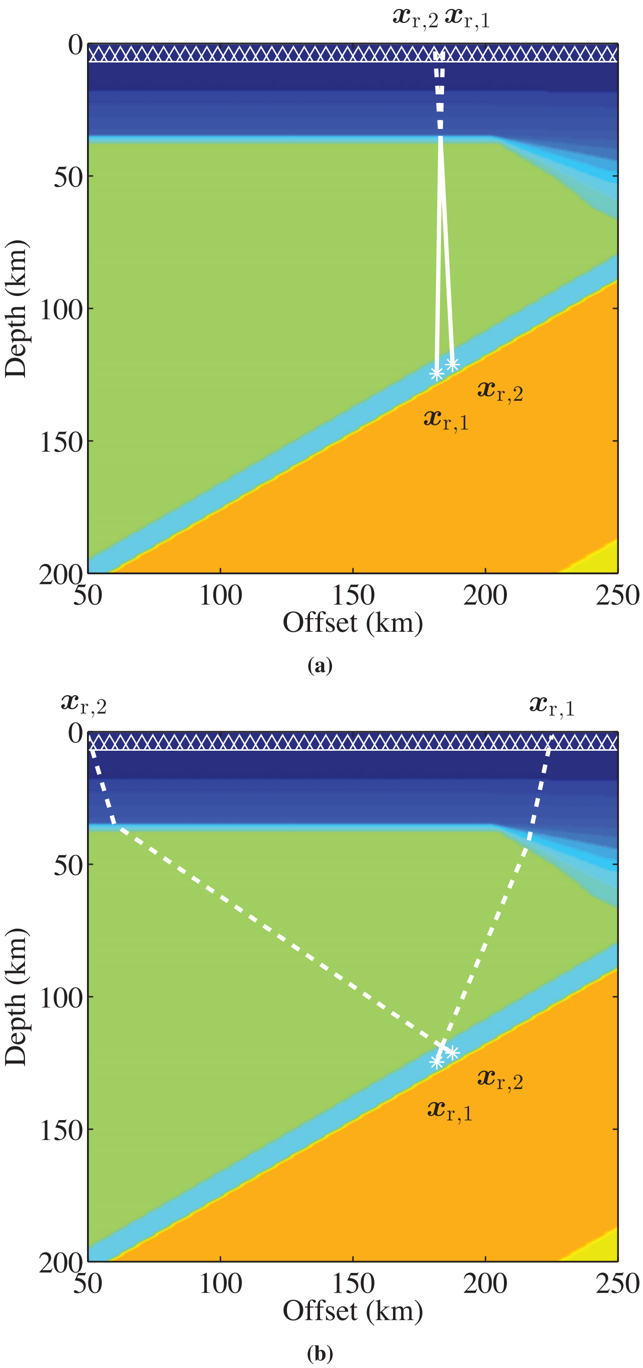

Figure 9. Redatuming surface-side reflections from (a) the overriding Moho and (b) the subducted interface down to source locations using source–receiver wavefield interferometry. The background is the velocity. Underside reflections are obtained by adding direct arrivals and subtracting the surface-side reflection. Again the dashed path is removed with our method, leaving the solid raypath.

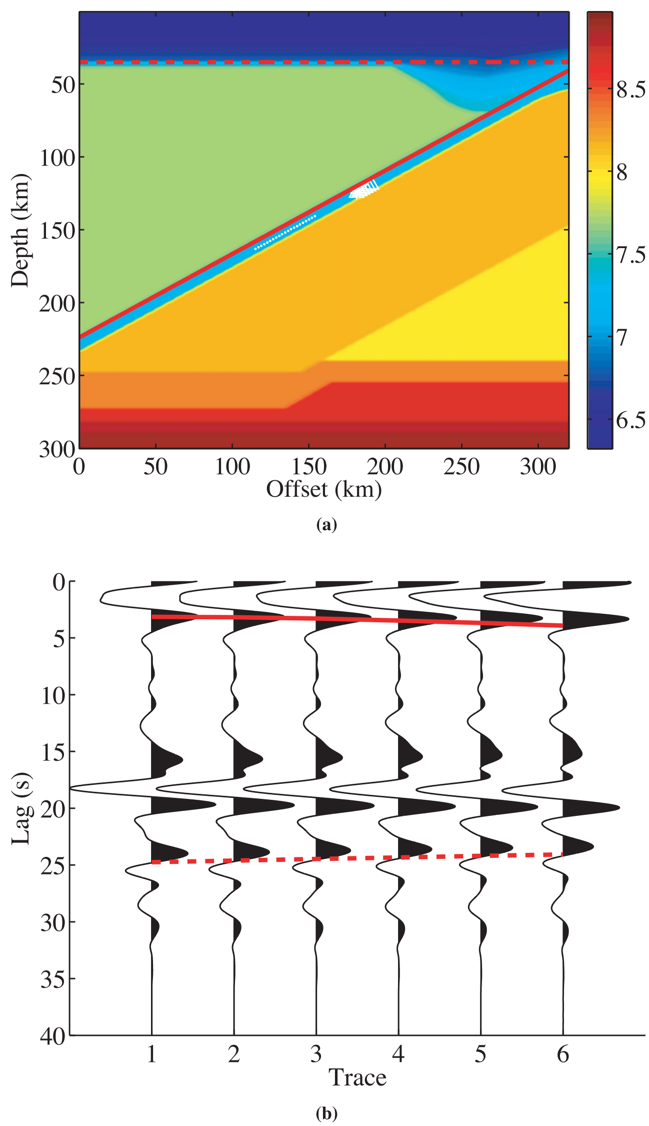

Figure 10. (a) The virtual source is placed at $x = 181$ km, and the virtual receivers span the offsets from 181 to 191 km. The illumination is restricted to sources that are at offsets from 115 to 154 km. (b) The reflection from the subducting crust (red solid line) is well recovered (compare with Fig. 8b). Other events are not physical.

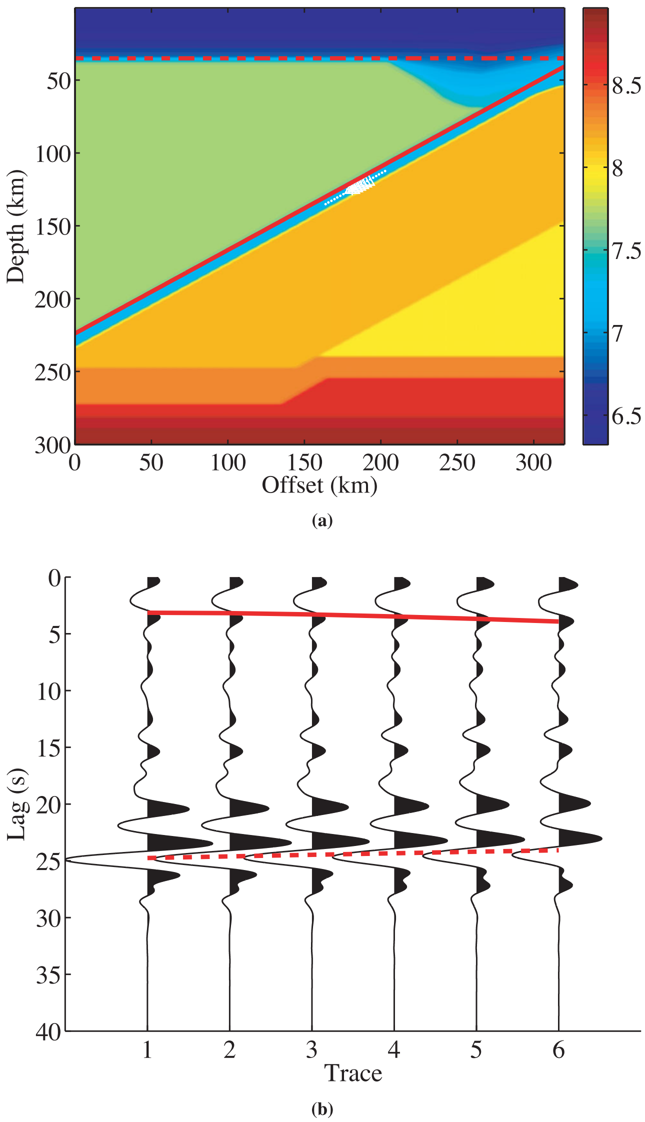

Figure 11. (a) The virtual source is placed at $x = 181$ km, and the virtual receivers span the offsets from 181 to 191 km. The illumination is restricted to sources that are at offsets from 163 to 202 km. (b) The reflection from the overriding crust (red dashed line) is well recovered (compare with Fig. 8b). Other events are not physical.

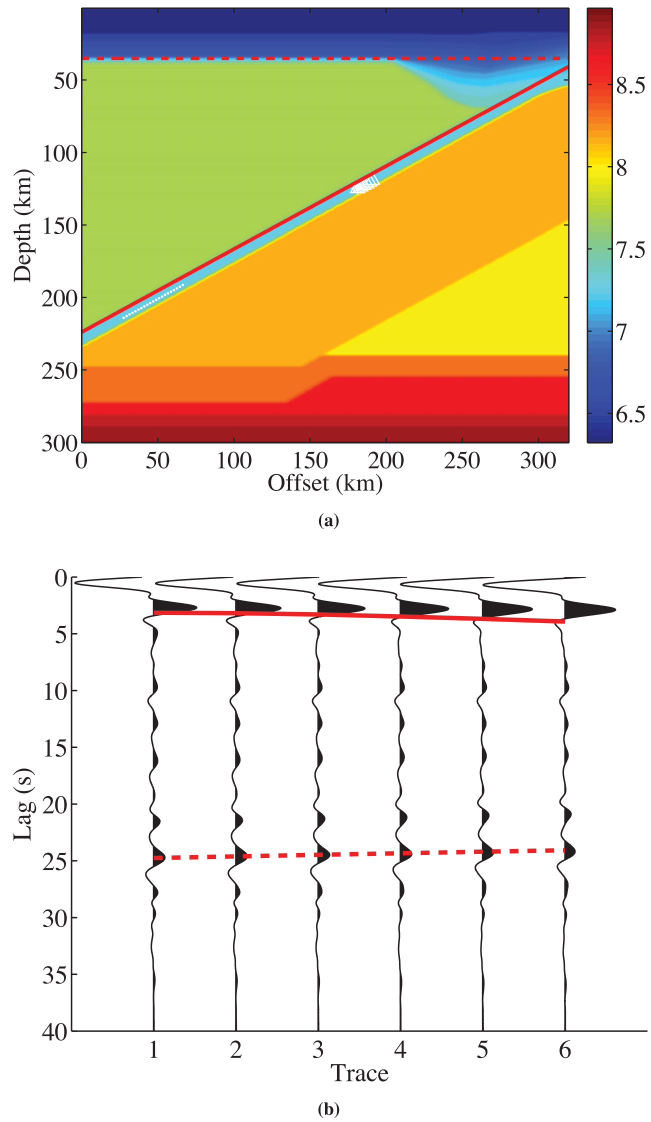

Figure 12. (a) The virtual source is placed at $x = 181$ km, and the virtual receivers span the offsets from 181 to 191 km. The illumination is restricted to sources that are at offsets from 27 to 66 km. (b) No event is reconstructed correctly as evidenced by the comparison with Fig. 8(b).

illumination is restricted to the sources positioned at offsets 163–202 km, as shown in Fig. 11, then we can recover the reflection from the overriding crust. Finally, Fig. 12 shows a window of sources with offsets from 27 to 66 that does not contain stationary events and, hence, the desired events cannot be reconstructed or have non-physical moveouts.

5 DISCUSSION

Our novel seismic redatuming method was validated using synthetic data computed for a complicated elastic model. When applying the algorithm to real data we should be prepared to meet additional challenges. They can be divided into several groups: the treatment of the seismic wavefield, the unknown source signature, the distribution of events and array receivers, the presence of multiples in the recorded data and the presence of refractions. The significance of these challenges may vary from one data set to another. In the remainder of this section, we discuss how these issues may be addressed in applications of our methodology to real data.

The simulations shown above use sources that have the same signature. This is not the case for real earthquakes. However, earthquakes are recorded by large arrays, and their source mechanisms can be recovered and inverted using redundancy in the array data. Deconvolving the source signature should then be relatively straightforward using, for example, the method proposed by (Chen *et al.* 2010). After this pre-processing step, the method would apply directly.

Numerous studies of various subduction zones have shown that the local seismicity inside the Wadati–Benioff zone is distributed roughly uniformly. We, thus, expect to obtain good-quality correlograms when applying our method in practice. Furthermore, as shown in the previous section, to locally image a specific interface it may be sufficient to have a relatively small cluster of strong events. Also, if gaps in events are found in correlograms then we could use the interferometric correlogram analysis discussed in Poliannikov & Willis (2011) to interpolate correlogram events where gaps are found and thus improve the final virtual gathers. We would also use teleseismic events in addition to the local earthquake data to build a virtual surface seismic survey. By including both types of events, we could obtain a richer data set with better illumination and signal-to-noise ratio.

In a related matter, the proposed technique assumes that the surface array of receivers is sufficiently dense to be treated as continuous. This is a perfectly good assumption for a number of data sets known in the literature, including an array of broadband seismometers installed in Southern Greece as part of the IRIS-PASSCAL Medusa experiment (Suckale *et al.* 2009), or the dense seismic observation network above the Japan subduction zone (Hi-net; Obara 2002; Chen *et al.* 2005). For data recorded by sparse arrays additional processing steps of the type described above will be necessary.

The realistic velocity model employed for illustration of our method contains some simplifications. The overriding crust, for example, may contain interfaces that introduce surface-related and internal multiples to the recorded data, particularly at higher frequencies. These multiples may contaminate the reflections from the subducted interfaces and create artefacts in their images. Theory suggests that the problem of surface-related multiples from the overriding plate should be well managed by constructing the virtual surface reflection survey interferometrically as we do in our method. Understanding the full effect of the multiples on the redatuming algorithm requires further investigation.

The spatial interpretation of the virtual gather obtained with any interferometric technique requires knowledge of the virtual acquisition. Because the locations of the earthquakes that are used as virtual receivers may contain their own uncertainty, constructing a space-image of the reflectors is a challenge. However, some interpretation can be done in the time domain. We can compare images obtained with traditional imaging method with ones obtained using the interferometric redatuming and check for consistency as well as rule out velocity anomalies in the overburden.

Finally, we note that our method, including the stationary phase analysis, deals only with reflections. Although it is possible to extend the method to include refractions, the resulting requirements on acquisition would likely be impractical in most conceivable scenarios. We expect the method to work well if the virtual receiver located in a low velocity layer is sufficiently close to the source to record a reflection. When the critical distance is exceeded, the method will break.

6 CONCLUSIONS

Obtaining a high-resolution image of a subducting interface remains an important problem. Traditional images constructed either by seismic reflections or teleseismic converted waves carry the imprint of velocity uncertainty accumulated over a considerable depth. A virtual gather constructed close to the interface would not have this problem and could be used to create a finer scale image.

Seismic interferometry has provided multiple methods of redatuming physically recorded data to a source or receive location. Each method has theoretical and practical requirements that need to be satisfied to produce a virtual gather containing a reliable image of the structure of interest. Neither classical interferometry nor source–receiver wavefield interferometry alone are well suited to solve our problem.

In this paper, we have laid out the theoretical framework for a novel methodology for obtaining an underside reflection off a structure of typical subduction zones using passive earthquake data recorded at the surface. We proposed a two-step algorithm of constructing a virtual gather at the location of one earthquake using data from multiple earthquakes. The first step consists of redatuming the earthquake events to the surface array using classical interferometry. In the second step, surface-side reflections were redatumed under the subducting interface using a known flavour of source–receiver wavefield interferometry. Ray geometry, acquisition setup and the location of the virtual gather together control the ultimate success of this technique.

ACKNOWLEDGMENTS

The authors would like to thank Xinding Fang of MIT for sharing his code for finite-difference modelling of elastic wave propagation. They would also like to thank Alison Malcolm, Yingcai Zheng, Pierre Gouédard and Maria Silva of MIT for helpful discussions of this work, and Kees Wapenaar of TU Delft and Andrew Curtis of University of Edinburgh for thoughtful reviews. This work was funded by the Earth Resources Laboratory Founding Member Consortium. Stéphane Rondenay was also supported by NSF grants: Continental Dynamics EAR-0409373 and Earthscope EAR-0544996. Ling Chen was supported by the National Science Foundation of China (Grant 90814002) and K.C. Wong Education Foundation, Hong Kong.

REFERENCES

Abers, G.A., MacKenzie, L.S., Rondenay, S., Zhang, Z., Wech, A.G. & Creager, K.C., 2009. Imaging the source region of Cascadia tremor and intermediate-depth earthquakes, *Geology,* **37,** 1119–1122.

Bakulin, A., Mateeva, A., Mehta, K., Jorgensen, P., Ferrandis, J., Herhold, I.S. & Lopez, J., 2007. Virtual source applications to imaging and reservoir monitoring, *Leading Edge,* **26,** 732–740.

Calvert, A.J., 2004. Seismic reflection imaging of two megathrust shear zones in the northern Cascadia subduction zone, *Nature,* **428,** 163–167.

Campillo, M. & Paul, A., 2003. Long-range correlations in the diffuse seismic coda, *Science,* **299,** 547–549.

Chen, C.-W., Miller, D.E., Djikpesse, H., Haldorsen, J.B.U. & Rondenay, S., 2010. Array-conditioned deconvolution of multiple-component teleseismic recordings, *Geophys. J. Int.,* **182,** 967–976.

Chen, L., Wen, L. & Zheng, T., 2005. A wave equation migration method for receiver function imaging: 2. application to the Japan subduction zone, *J. geophys. Res.,* **110,** B11310–B11325.

Curtis, A., 2009. Source-receiver seismic interferometry, *SEG Expanded Abstr.*, **28**, 3655–3658, doi:10.1190/1.3255626.

Curtis, A. & Halliday, D., 2010. Source-receiver wavefield interferometry, *Phys. Rev. E,* **81,** 046601-1-046601-10.

Curtis, A., Nicolson, H., Halliday, D., Trampert, J. & Baptie, B., 2009. Virtual seismometers in the subsurface of the Earth from seismic interferometry, *Nat. Geosci.,* **2,** 700–704.

Derode, A., Larose, E., Campillo, M. & Fink, M., 2003. How to estimate the Green's function of a heterogeneous medium between two passive sensors? Application to acoustic waves, *Appl. Phys. Lett.,* **83**. 3054–3056.

Husen, S., Quintero, R., Kissling, E. & Hacker, B., 2003. Subduction-zone structure and magmatic processes beneath Costa Rica constrained by local earthquake tomography and petrologic modeling, *Geophys. J. Int.,* **155,** 11–32.

MacKenzie, L.S., Abers, G.A., Rondenay, S. & Fischer, K.M., 2010. Imaging a steeply dipping subducting slab in Southern Central America, *Earth planet. Sci. Lett.,* **296,** 459–468.

Mehta, K., Snieder, R., Calvert, R. & Sheiman, J., 2008. Acquisition geometry requirements for generating virtual-source data, *Leading Edge,* **27,** 620–629.

Obara, K., 2002. Nonvolcanic deep tremor associated with subduction in Southwest Japan, *Science,* **296,** 1679–1681.

Poliannikov, O.V., 2011. Retrieving reflections by source-receiver wavefield interferometry, *Geophysics,* **76,** SA1–SA8.

Poliannikov, O.V. & Willis, M.E., 2011. Interferometric correlogram-space analysis, *Geophysics,* **76,** SA9–SA17.

Preston, L.A., Creager, K.C., Crosson, R.S., Brocher, T.M. & Trehu, A.M., 2003. Intraslab earthquakes: dehydration of the Cascadia slab, *Science,* **302,** 1197–1200.

Rickett, J. & Claerbout, J., 1996. *Passive Seismic Imaging Applied to Synthetic Data* Technical Report 92, Stanford Exploration Project, available at http://sepwww.stanford.edu/public/docs/sep92/james1.ps.gz (last accessed 2012 February 12).

Rondenay, S., Bostock, M. & Shragge, J., 2001. Multiparameter two-dimensional inversion of scattered teleseismic body waves 3. Application to the Cascadia 1993 data set, *J. geophys. Res.,* **106,** 30 795–30 807.

Schuster, G.T., 2009. *Seismic Interferometry,* 2nd edn, Cambridge University Press, Cambridge.

Schuster, G.T., Yu, J., Sheng, J. & Rickett, J., 2004, Interferometric/daylight seismic imaging, *Geophys. J. Int.,* **157,** 838–852.

Schuster, G.T. & Zhou, M., 2006. A theoretical overview of model-based and correlation-based redatuming methods, *Geophysics,* **71,** SI103–SI110.

Shelly, D.R., Beroza, G.C., Zhang, H., Thurber, C.H. & Ide, S., 2006, High-resolution subduction zone seismicity and velocity structure beneath Ibaraki Prefecture, Japan, *J. geophys. Res.,* **111,** B06311–B06320.

Snieder, R., 2004. Extracting the Green's function from the correlation of coda waves: a derivation based on stationary phase, *Phys. Rev. E,* **69,** 046610.1–046610.8.

Stachnik, J.C., Abers, G.A. & Christensen, D.H., 2004. Seismic attenuation and mantle wedge temperatures in the Alaska subduction zone, *J. geophys. Res.,* **109,** B10304.

Suckale, J., Rondenay, S., Sachpazi, M., Charalampakis, M., Hosa, A. & Royden, L.H., 2009. High-resolution seismic imaging of the western Hellenic subduction zone using teleseismic scattered waves, *Geophys. J. Int.,* **178,** 775–791.

The ANCORP Working Group, 1999. Seismic reflection image revealing offset of Andean subduction-zone earthquake locations into oceanic mantle, *Nature,* **397,** 341–344.

Wagner, L.S., Beck, S. & Zandt, G., 2005. Upper mantle structure in the south central Chilean subduction zone (30° to 36° S), *J. geophys. Res.,* **110,** B01308–B01327.

Wapenaar, K., 2004. Retrieving the elastodynamic Green's function of an arbitrary inhomogeneous medium by cross correlation, *Phys. Rev. Lett.,* **93,** 254301-1-4.

Wapenaar, K., Fokkema, J.T. & Snieder, R., 2005. Retrieving the Green's function in an open system by cross correlation: a comparison of approaches, *J. acoust. Soc. Am.,* **118,** 2783–2786.

Wiens, D.A., Conder, J.A. & Faul, U.H., 2008. The seismic structure and dynamics of the mantle wedge, *Annu. Rev. Earth and Planet. Sci.,* **36,** 421–455.

Zhang, H. & Thurber, C.H., 2006. Development and applications of double-difference seismic tomography, *Pure appl. Geophys.,* **163,** 373–403.